https://www.aimspress.com/journal/mine

Mathematics in Engineering, 7(5): 586–609.
DOI:10.3934/mine.2025024
Received: 09 January 2025
Revised: 19 May 2025
Accepted: 01 September 2025
Published: 11 September 2025

Research article

Identification of the parameters of the stochastic Preisach operator†

Aleksandr I. Proshunin[1,*], Sergei V. Borzunov[1] and Nikolay I. Sel'vesyuk[2]

[1] Digital Technologies Department, Voronezh State University, Universitetskaya sq. 1, Voronezh 394006, Russia

[2] State Research Institute of Aviation Systems, Viktorenko st. 7, Moscow 125319, Russia

† **This contribution is part of the Special Issue:** Multi-Rate Processes and Hysteresis
Guest Editors: Menita Carozza; Dmitrii Rachinskii; Ciro Visone
Link: www.aimspress.com/mine/article/6692/special-articles

* **Correspondence:** Email: alexfrauch@gmail.com.

Abstract: In this paper, we propose a method for identifying the measure of the stochastic Preisach operator using machine learning techniques. The classical Preisach operator model is widely used to describe hysteresis phenomena in various fields such as physics, chemistry, economics, and biology. However, it does not account for uncontrolled fluctuations in the parameters of elementary hysteresis carriers — hysterons, which limits its applicability in real systems where these parameters can be stochastic variables. The proposed method is based on sequential reconstruction of the operator's measure on the plane of hysteron threshold parameters (α, β). The identification is carried out through specially constructed input signals that trigger switching of only specific hysterons in given local regions of this plane. Multiple repetitions of such input actions and application of the law of large numbers allow for estimating the mathematical expectations of hysteron state changes. These estimates are used in the algorithm to minimize a loss functional, leading to the reconstruction of the operator's measure from experimental data. The results open new possibilities for modeling and analyzing complex systems with hysteretic properties, taking into account the stochastic nature of parameters.

Keywords: stochastic Preisach operator; machine learning; identification of Preisach operator parameters; non-ideal relays; complex systems modeling

1. Introduction

As is well known, hysteresis is a phenomenon observed in various fields of physics, chemistry, economics, and biology. A distinctive feature of hysteresis operators is the fact that their output at the

current moment in time depends on the initial state and the input values at all previous moments in time. Typically, carriers of hysteresis properties are part of higher-level systems. Therefore, modern hysteresis models allow for their integration into such systems.

Mathematical models of dynamic systems with hysteresis components can be described using the technique of operator-differential equations, where hysteresis elements correspond to operators that depend on their initial state as a parameter and are defined on a broad functional space. The possibility of such an interpretation of hysteresis nonlinearities is based on the operator approach to modeling hysteresis operators developed by M. A. Krasnoselskii and his students [41] within the framework of system theory.

Ideas related to the description of ferromagnetic hysteresis through systems of non-ideal relays date back to the work [20]. In 1935, Franz Preisach proposed a clear geometric interpretation of a continuous system of non-ideal relays, which forms the basis of the ferromagnetic hysteresis model [52]. In this regard, we note the work [71], where the existence of hysterons (Preisach particles) in ferroelectrics was experimentally confirmed. However, the classical Preisach model does not account for uncontrollable fluctuations of elementary hysteresis carriers—non-ideal relays. To date, the Preisach model is one of the most popular constructive models successfully applied for modeling hysteresis effects in various subject areas [21–23, 38, 56, 59, 63–65, 67].

In the work [14], a model was considered in which the carrier of hysteresis properties, possessing a domain structure, exhibited "not quite" deterministic behavior. This study demonstrated that the hysteresis loop at each stage of magnetization experienced uncontrollable variations (while the experimental conditions ensured almost perfect constancy of external conditions such as temperature, pressure, etc.). Similar results, including those for ferroelectrics polarized by a periodically changing electric field, are presented in the works [51, 76]. This implies that classical models (both phenomenological and constructive) can be considered only as a "first approximation" in the tasks of parameter identification for systems with ferromagnetic and ferroelectric hysteresis.

In the works [5, 6, 66], the authors generalize the Preisach and backlash models to the case where the parameters of elementary hysteresis carriers are stochastic variables. In this context, the output of the corresponding operators is treated as a stochastic process whose parameters, in turn, are determined by the parameters and initial state of the hysteresis operators. For this stochastic process, the first and second statistical moments are obtained explicitly.

Ferromagnetic and ferroelectric materials exhibit nonlinear dependencies and hysteresis effects due to the peculiarities of their internal structure, such as magnetic domains in ferromagnets and domain regions in ferroelectrics. In ferromagnets, there is a complex dependence of magnetization M on the external magnetic field H, associated with the rotation of the magnetization vector and changes in the size and number of domains, which is described by the Preisach, Jiles–Atherton, and Stoner–Wohlfarth models [34, 69]. Similarly, ferroelectrics demonstrate spontaneous polarization and a nonlinear dependence of electric displacement on the external electric field, actively utilized in actuators, energy storage devices, as well as in non-volatile memory and RFID cards [12, 27]. The Preisach model is widely used to describe hysteresis phenomena in these materials [10, 11, 15, 19, 30, 37]; however, to account for dynamic effects and improve modeling accuracy, its generalizations have been developed, incorporating the dependence of functions on the rate of change of input data and the history of changes [44, 54, 75].

We specifically highlight the fundamental monograph [40, 45, 46], where a generalization of the

Preisach model is considered for the case when the input is represented as a sum of deterministic and stochastic components. As the author points out, this model is particularly important in situations involving thermal fluctuations of the medium exhibiting hysteretic properties. The author demonstrates that the stochastic input is consistent with shifts in the threshold values of non-ideal relays, with such shifts occurring for both threshold values. The work provides an effective tool for extracting the expectation of the output under the assumption that the noise is modeled by an i.i.d. process. The obtained results are compared with thermal activation-type models for viscosity. One of the important conclusions presented in this work is the independence of the asymptotic output from the input history, as well as the insensitivity to variations in the stochastic component. In other words, in the approach described in [45], stochastic fluctuations of threshold values are synchronized, whereas the present work considers a model in which stochastic fluctuations of threshold values of non-ideal relays are independent.

Direct and inverse piezoelectric effects, as well as technical systems based on them, find wide application in industry, including quartz resonators, piezo transformers, microphone and hydrophone sensors, piezoceramic emitters, and precision positioning systems [1, 31, 42, 47, 60]. In recent years, significant progress in energy harvester converters [7, 18, 43, 73] has highlighted the role of nonlinear and hysteresis effects in device efficiency. The Preisach model has proven practical significance in describing hysteresis phenomena, including hysteresis compensation in smart actuators [32, 33], modeling nonlinear hysteresis effects in energy storage [9, 13, 16, 65], parameter identification of hysteresis models [8, 25, 39, 55], multi-level non-volatile memory [36, 71], analysis of complex networks [35], and energy source modeling [2, 3, 72].

The present work is dedicated to developing a method for identifying the measure of the Preisach operator under conditions of stochasticity in the parameters of elementary hysterons using machine learning methods.

2. Methodology

The generalization of the Preisach operator, which assumes the stochasticity of the parameters of its constituent non-ideal relays, is presented in [6], where the corresponding definition is provided, along with a description of its probabilistic characteristics in terms of the moment functions of the output.

We provide a brief description of the corresponding operator: A non-ideal relay with stochastic threshold values $R[p_0, \hat{\alpha}, \hat{\beta}, x_0, t_0]$ is understood as an operator that maps a continuous input into an output–a stochastic process. Here, $\hat{\alpha}, \hat{\beta}$ are continuous stochastic variables with known probability distributions.

It is further assumed that all continuous $u(t)$ $(t \geqslant t_0)$ are permissible for the stochastic relay operator. The space of possible states of the operator is defined as $\Omega = \Omega(\{0, 1\},\ 0 \leqslant p(t) \leqslant 1,\ u \in \mathbb{R})$.

At each fixed moment in time t, we define the variable state of the operator as the pair $\{u(t),\ p(t)\}$, and the output as the stochastic process $R[p_0, \hat{\alpha}, \hat{\beta}, x_0, t_0]u(t)$, which takes the value $+1$ with probability $p(t)$ and the value -1 with probability $(1 - p(t))$. (Note that quite often the output values of the non-ideal relay are taken to be 0 and 1; in this case, it is quite obvious that the transition from one operator to another is achieved by a simple affine transformation.) In other words, $P\{R[p_0, \hat{\alpha}, \hat{\beta}, x_0, t_0]u(t) = 1\} = p(t)$.

The evolution of the probability $p[p_0, u(\tau)|_{t_0 \leqslant \tau \leqslant t}](t)$ for monotonic input signals, when $t \geqslant t_0$, is as

follows:

$$p[p_0, u(\tau)|_{t_0\leqslant\tau\leqslant t}](t) = \begin{cases} \max\left[p_0,\ \int_{-\infty}^{u(t)} \varphi_\beta(u)\,du\right], & \text{if } u(t) \text{ increases,} \\ \min\left[p_0,\ \int_{-\infty}^{u(t)} \varphi_\alpha(u)\,du\right], & \text{if } u(t) \text{ decreasing.} \end{cases}$$

For piecewise-monotonic input signals, the dynamics of the operator are determined using the semigroup property, and for arbitrary continuous input signals, by a limiting process in which any continuous input is considered as the limit of continuous piecewise-monotonic inputs. The proofs of the correctness of the definition and the limiting process are provided in [6]. Analogous to the classical case, the concept and definition of a finite system of non-ideal relays with stochastic parameters, connected in parallel, is introduced (see Figures 1 and 2).

$$\xi_N\Big[p(t),\ \hat{\alpha},\ \hat{\beta},\ x_0,\ t_0,\ u(t)\Big] = \sum_{j=1}^{N} \mu_j\, R\Big[p_0,\ \hat{\alpha}_j,\ \hat{\beta}_j,\ x_0,\ t_0\Big]\, u(t). \tag{2.1}$$

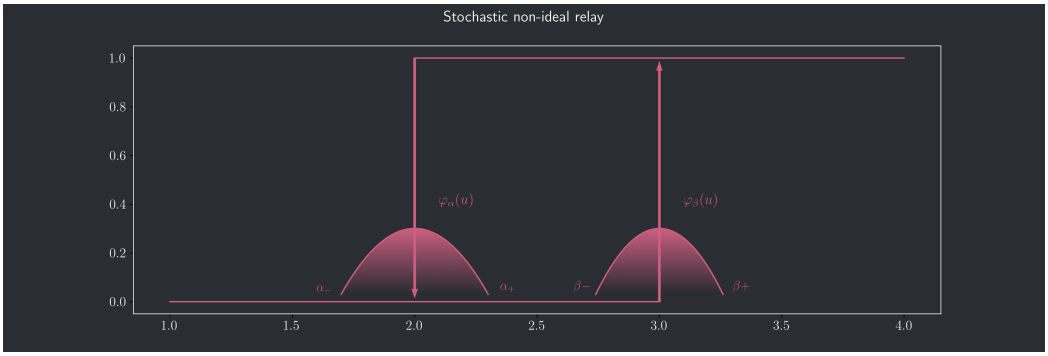

Figure 1. Non-ideal relay.

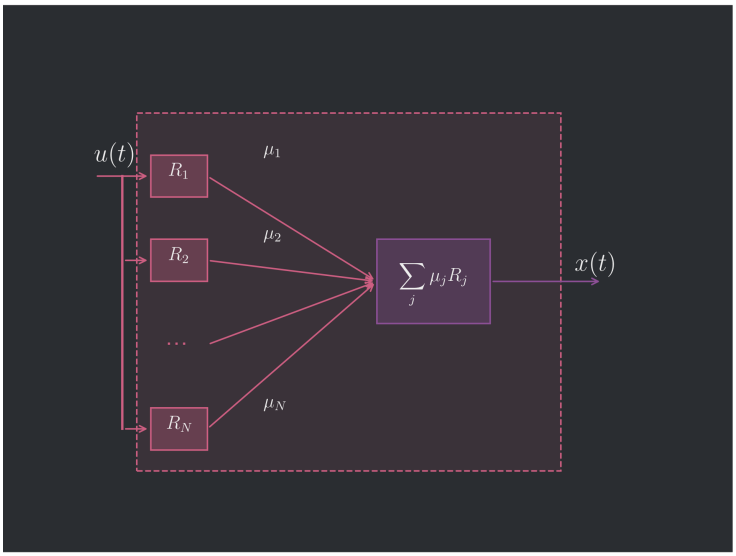

Figure 2. The parallel connection of N non-ideal relays $R_j\left[\alpha_j, \beta_j, x_0^{(j)}, t_0\right]$, each taken with weights $\mu_j > 0$, where $j = 1, \ldots, N$.

The stochastic Preisach operator is defined by transitioning to a continuous limit in the formula (above), as μ_j tend to zero proportionally to the areas of elementary regions on the half-plane $\beta > \alpha$. The state space of the specified operator consists of pairs $(\phi, u(t))$, where the first component ϕ is a function that takes the value $+1$ at a point on the half-plane $\beta > \alpha$ with probability $P(\alpha, \beta)$ and -1 with probability $1 - P(\alpha, \beta)$.

The dynamics of the stochastic Preisach operator are determined by the input-state and state-output:

$$f(t) = \hat{\Gamma} u(t) = \iint_{\beta > \alpha} \mu(\alpha,\ \beta) R\left[p_0,\ \hat{\alpha},\ \hat{\beta},\ x_0,\ t_0\right] u(t)\, d\alpha\, d\beta.$$

In practical applications, it is extremely important to identify the measure of the Preisach operator based on data from a relatively small number of experiments, which involve observing input-output pairs. Typically, this involves identifying the parameters of a discrete analogue of the Preisach operator 2.1. In the context of the case under consideration, this means that the function $\mu(\alpha, \beta)$, which determines the contribution of individual relays to the output of the Preisach operator, can be approximated with sufficient accuracy by a piecewise constant function (it is known that any continuous function on a closed bounded set can be approximated with any desired accuracy by a piecewise constant function). Moreover, in the case under consideration, it is assumed that the support of the Preisach operator's measure is divided into rectangular or triangular subregions (adjacent to the line $\alpha = \beta$), where the function $\mu(\alpha, \beta)$ is considered constant. In the case of the stochastic Preisach operator, the identification task is significantly complicated for obvious reasons. Figure 3 shows the input-output relationship of the discrete analogue of the stochastic Preisach operator for a periodic input. As can be seen from the figure, there is a "blurring" of the hysteresis loop caused by the influence of stochastic factors.

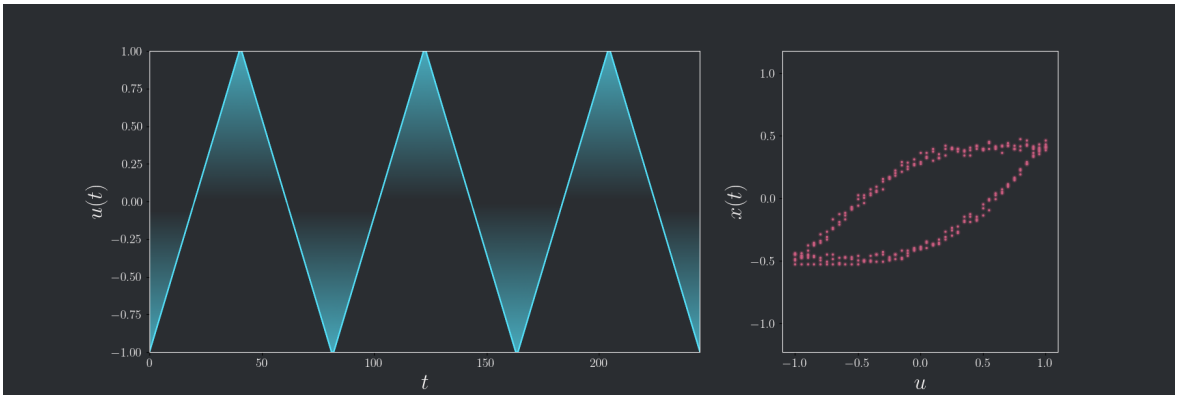

Figure 3. Dependence of the output signal on the input $u(t)$.

2.1. Identification algorithm

To experimentally retrieve information about the distribution function $\mu(\alpha, \beta)$, Mayergoyz proposed a specialized protocol involving measurements of partial hysteresis loops known as First Order Reversal Curves (FORC) [46]. Each FORC is obtained as follows: the sample is initially driven into saturation (for instance, by applying a sufficiently large positive field so that all hysterons are in state

+1). Subsequently, the field is monotonically decreased to a certain value H_b (the reversal field, i.e., the reversal point). Upon reaching H_b, the field direction is reversed, and the field is increased back towards positive saturation. The magnetization trajectory $M(H)$ obtained from H_b to saturation constitutes the FORC associated with the point H_b on the descending branch of the main hysteresis loop [57]. By repeating this experiment for a range of H_b values (forming a family of FORCs), data $M(H_a, H_b)$—the magnetization for the applied field H_a after reversal at level H_b—can be collected, where H_a varies from H_b to saturation. Thus, $M(H_a, H_b)$ is defined within the region $H_a \geq H_b$ (analogous to the Preisach triangle) and represents the surface of partial loops (occasionally referred to as the Everett surface). The connection between FORC and the Preisach model is that $M(H_a, H_b)$ encodes information about the distribution of hysterons. Intuitively, the choice of H_b and H_a determines which hysterons have switched states.

In the ideal case, the function $M(H_a, H_b)$ is smooth and differentiable, related to the measure $\mu(\alpha, \beta)$ by the fundamental equation:

$$\mu(\beta, \alpha) = \frac{1}{2} \frac{\partial^2 M(H_a = \alpha, H_b = \beta)}{\partial H_b \partial H_a},$$

evaluated at the point (α, β).

Mayergoyz's Classical Method (direct differentiation). In practice, this implies:

(1) Conducting a series of FORC measurements to obtain discrete values of $M(H_a, H_b)$.

(2) Approximating experimental data with a smooth surface $f(\beta, \alpha) \approx M(H_a = \alpha, H_b = \beta)$.

(3) Numerically differentiating this function to estimate $\mu(\beta, \alpha)$.

However, direct differentiation is problematic due to noise and data discreteness. Typically, smoothing or fitting the surface precedes differentiation. Hughes and Wen [29] approximated $f(\beta, \alpha)$ using bivariate polynomials fitted via least squares. Gorbet et al. [24] suggested special functional approximations with weighted least squares fitting. A key difficulty is sensitivity to the approximation chosen; as Gorbet et al. noted, differentiation of fitted surfaces is inherently inaccurate, and different approximations yield notably different $\mu(\alpha, \beta)$ distributions. Nevertheless, Mayergoyz's FORC method has established itself as effective, particularly for near-Preisach hysteresis behavior.

Integral equations approach (direct method without differentiation). Hoffmann and Sprekels [28] proposed directly retrieving $\mu(\alpha, \beta)$ by solving integral equations that relate measured M values to hysteron distributions. This method discretizes the Preisach plane and formulates linear equations regarding discrete masses μ_{ij}. These equations, solved iteratively or in blocks, avoid explicit differentiation. Later developments by Hoffmann and Meyer refined the approach, approximating $\mu(\alpha, \beta)$ through basis functions determined by discrete data. Direct methods are appealing due to avoiding numerical differentiation but suffer significant sensitivity to measurement errors, often necessitating regularization.

Identification from Limited Data and Other Approaches. Recognizing that a complete FORC dataset is extensive, attempts have been made to simplify the procedure. For example, Galinaitis and Rogers suggested stimulating systems with rich signals and identifying μ from limited response data. Artificial intelligence methods, such as neural networks trained on limited hysteresis data, have also been explored, although these remain outside standard methodologies. Still, comprehensive FORC measurements remain the most informative approach for distribution recovery [17, 26, 53, 61].

Smoothing and Regularization. Given the sensitivity of direct differentiation to noise, data smoothing and regularization methods are essential. Early studies manually approximated $f(\beta, \alpha)$,

while modern automated algorithms, such as the LOESS smoothing developed by Harrison and Feinberg [26], are widely used. Egli [17] introduced the VARIFORC method, adaptively varying smoothing intensity across the FORC diagram. Regularization, such as Tikhonov regularization, addresses ill-posed differentiation problems, ensuring physically realistic, stable solutions from noisy data.

In conclusion, the FORC method is deeply established as a robust and informative experimental procedure for Preisach distribution reconstruction, underpinned by Mayergoyz's elegant mathematical foundation. Its development from manual approximation to sophisticated automated smoothing algorithms reflects its broad application in hysteresis research and practical engineering applications [4, 24, 50, 53, 57]. It is important to note that the applicability of classical FORC analysis is limited to systems that closely approximate ideal Preisach behavior. Nevertheless, even in cases of deviation, FORC diagrams provide a valuable "fingerprint" of the material's hysteretic properties, helping to decompose complex responses into constituent components and guiding the development of more accurate models [68, 70, 74]. In physics and materials science, the FORC method has established itself as an informative experimental approach, and its combination with the mathematical rigor of the Preisach model makes it a powerful tool for both fundamental research and practical engineering applications.

The main idea of identifying the measure of the stochastic Preisach operator lies in the sequential reconstruction of the measure over the region of the (α,β)-plane corresponding to the hysteresis support. This is achieved by moving along the triangle $\beta \geq \alpha$ from bottom to top and right to left.

The identification process is based on the application of specific input signals that trigger switching only in certain elementary hysterons (imperfect relays) within a given local parameter region (α,β). Repeated application of such input signals and the use of the law of large numbers allow for the estimation of the expected change in the state of these hysterons, as well as the determination of the measure value $\mu(\alpha,\beta)$ in the given region.

2.2. Step-by-step description of the method

The procedure for identifying the measure is constructed step-by-step, starting from the regions of the triangle $\beta \geq \alpha$ with the smallest values of α and the largest values of β, and sequentially moving upwards and to the left, covering the entire support region of the measure.

2.2.1. Initialization of the right lower region

- **Step 1:** Set the input signal $u(t)$ to the value $\beta_{\max}$, corresponding to the right lower corner of the triangle on the (α,β)-plane.
- **Step 2:** Decrease the input signal to the value $\beta_{\max}-\Delta\beta$ to turn off all hysterons with $\beta \geq \beta_{\max}-\Delta\beta$.
- **Step 3:** Increase the input signal to the value $\alpha_{\max}$, where $\alpha_{\max} = \beta_{\max} - \Delta\beta$. This turns on hysterons with $\alpha \leq \alpha_{\max}$.
- **Step 4:** Record the change in the output signal $\Delta f(t)$.

This sequence of input actions allows focusing on the region $[\alpha_{\max} - \Delta\alpha, \alpha_{\max}] \times [\beta_{\max} - \Delta\beta, \beta_{\max}]$, causing the switching of hysterons specifically in this area. Visualization of this algorithm is presented in Figure 4.

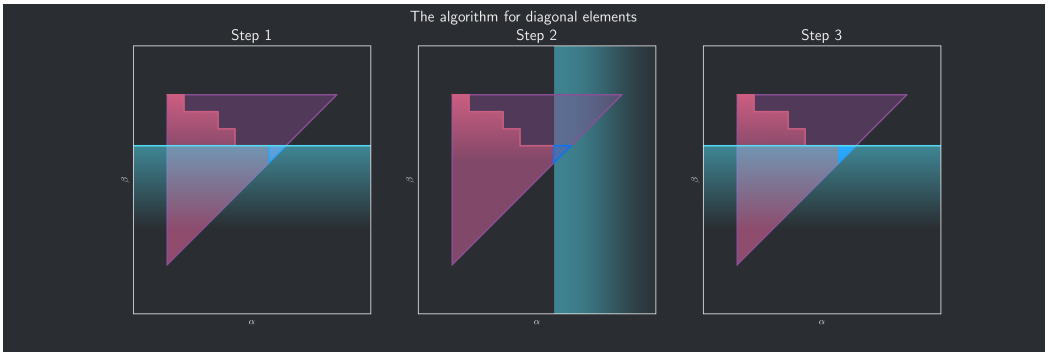

Figure 4. An algorithm for obtaining a change in a certain area of the Preisach operator.

2.2.2. Iterative horizontal update from right to left

- **Step 1:** Move to the next value $\alpha_i = \alpha_{\max} - i\Delta\alpha$, where $i = 1, 2, \ldots$.
- **Step 2:** Repeat the sequence of input actions:
  - Set $u(t) = \beta_j$ (current value of β).
  - Decrease $u(t)$ to $\beta_j - \Delta\beta$.
  - Increase $u(t)$ to α_i.
  - Record the change in output $\Delta f_{i,j}$.
- **Step 3:** Calculate the expected value $E[\Delta f_{i,j}]$ for the region $[\alpha_i - \Delta\alpha, \alpha_i] \times [\beta_j - \Delta\beta, \beta_j]$.
- **Step 4:** Update the estimate of the measure $\mu(\alpha, \beta)$ in the current region.

Visualization of this algorithm is presented in Figure 5.

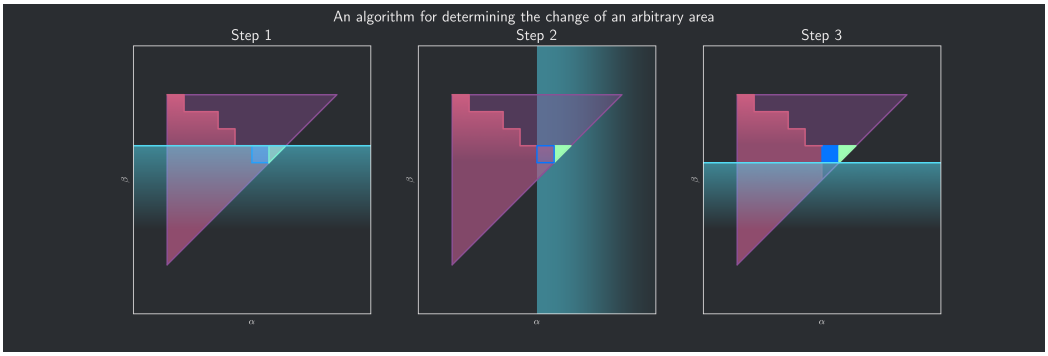

Figure 5. Algorithm for obtaining changes in a specific region of the Preisach operator.

2.2.3. Vertical progression from bottom to top

- After traversing all α values horizontally from right to left at a fixed β_j, proceed to the next value $\beta_{j+1} = \beta_j + \Delta\beta$.
- **Step 1:** Set the input signal $u(t) = \beta_{j+1}$.
- **Step 2:** Repeat the iterative horizontal update procedure for the new value β_{j+1}.

2.2.4. Moving across the triangle from bottom to top and right to left

Continue the process by moving from bottom to top (increasing β) and from right to left (decreasing α), sequentially covering the entire region of the triangle $\beta \geq \alpha$, as illustrated in the article.

At each step, record the changes in the output signal corresponding to local areas and update the estimate of the measure $\mu(\alpha, \beta)$ for these areas.

2.3. Mathematical expectation

For each local area $[\alpha_i - \Delta\alpha, \alpha_i] \times [\beta_j - \Delta\beta, \beta_j]$, the expected value of the change in the output signal for the corresponding input action is determined as:

$$E[\Delta f_{i,j}^{\exp}] = \frac{1}{n} \sum_{k=1}^{n} \Delta f_{i,j}^{\exp(k)}, \tag{2.2}$$

$$E[\Delta f_{i,j}^{\text{model}}] = \sum_{k} (p(\alpha_i, \beta_i | u(t + \triangle t)) \mu(\alpha_i, \beta_i) R\left[p_0, \hat{\alpha}, \hat{\beta}, x_0, t_0\right] u(t + \triangle t)$$
$$- p(\alpha_i, \beta_i | u(t)) \mu(\alpha_i, \beta_i) R\left[p_0, \hat{\alpha}, \hat{\beta}, x_0, t_0\right] u(t)).$$

The goal is to minimize the loss functionality:

$$\mathcal{L}(\mu) = \sum_{k} \left(E[\Delta f_{i,j}^{\exp(k)}] - E[\Delta f_{i,j}^{\text{model}(k)}(\mu)] \right)^2 \to \min_{\mu},$$

where:

- $E[\Delta f_{i,j}^{\exp}]$: The experimentally measured expected change in output in the region $[\alpha_i - \Delta\alpha, \alpha_i] \times [\beta_j - \Delta\beta, \beta_j]$;
- $E[\Delta f_{i,j}^{\text{model}}(\mu)]$: The model-based expected change in output, calculated with the current approximation of the measure μ.

2.4. Sequential measure update

When using optimization methods such as gradient descent, only the parameters of the measure $\mu(\alpha, \beta)$ in the current identification area are updated at each step. Gradients for already processed areas are set to zero:

$$\frac{\partial \mathcal{L}}{\partial \mu(\alpha, \beta)} = 0, \quad \text{if } (\alpha, \beta) \notin \text{current area}.$$

This allows focusing on optimizing the measure only in the current local area, minimizing the impact on previously identified parameters.

The proposed method for identifying the measure of the stochastic Preisach operator, based on moving across the triangle from bottom to top and right to left, enables efficient and accurate reconstruction of the measure distribution $\mu(\alpha, \beta)$ over the entire area of the triangle $\beta \geq \alpha$. This ensures the reliability and accuracy of modeling hysteresis systems based on the Preisach operator.

3. Theoretical justification

3.1. Mathematical formulation

Formally, the method can be viewed as the problem of minimizing a discrepancy functional (loss functional) between experimental and model responses across all local regions. Let $E[\Delta f_{i,j}^{\exp}]$ be the experimentally estimated expectation of the output change, obtained by averaging multiple observations for cell (i, j). This represents the target (true) response that the model should approximate. On the other hand, given some trial measure $\mu(\alpha, \beta)$, one can compute the model expected output change $E[\Delta f_{i,j}^{\text{model}}(\mu)]$ for the same input stimulus by integrating the current measure over cell (i, j) (considering the switching probabilities of hysterons given the measure μ). The algorithm aims to minimize the squared deviations between these values for all cells:

$$\mathcal{L}(\mu) \;=\; \sum_{k} \Big(E[\Delta f_{i,j}^{\exp}] - E[\Delta f_{i,j}^{\text{model}}(\mu)] \Big)^2 \;\to\; \min_{\mu}.$$

Here, $\mu = \{\mu_{ij}\}$ is the set of measure parameters for all cells to be identified. By minimizing $\mathcal{L}(\mu)$, we adjust the parameters μ_{ij} so that the model responses match the experimental ones, effectively reconstructing the measure from observations. The optimal solution μ^* to this problem is the true (unknown) operator measure that we aim to find.

In practice, minimization of $\mathcal{L}(\mu)$ is performed using stochastic gradient descent (SGD). After each local experiment, the algorithm updates the parameters by stepping in the direction opposite to the gradient of the current loss functional value. Only the parameter μ_{ij} of the currently processed cell is updated; gradients for other parameters are set to zero. Thus, one cycle scanning all regions (epoch) corresponds to one pass through all components of parameter μ, using SGD on batches of local observations.

Below, we demonstrate that under certain conditions on the stochastic nature of hysterons and proper selection of the update step, this algorithm converges to the true measure μ^*. We first state the theorem, specifying the conditions and the convergence claim, and then present its proof.

3.2. Convergence theorem of the method

Assumption 1. *(1) Properties of the measure and observations. The true Preisach operator measure $\mu^*(\alpha, \beta)$ is continuous and bounded over the triangular domain $\{\beta \geq \alpha\}$, and it is approximated by a parametric family $\mu(\alpha, \beta)$ (a piecewise-constant function over a given partition) without systematic error. The hysteron threshold values in each local region are assumed to be independent and identically distributed random variables with a fixed distribution (e.g., uniform or normal), possessing finite variance. This guarantees the applicability of the law of large numbers and ensures that experimental estimates converge to their expected values.*

(2) Properties of the loss functional. The functional $\mathcal{L}(\mu)$ is convex in the parameters μ_{ij} and has an L-Lipschitz continuous gradient (i.e., the gradient is continuous and satisfies $\|\nabla\mathcal{L}(\mu) - \nabla\mathcal{L}(\nu)\| \leq L\|\mu - \nu\|$ for all μ, ν). Moreover, $\mathcal{L}(\mu)$ is strongly convex – there exists a constant $z > 0$ such that for all admissible μ, ν the following strong convexity inequality holds:

$$\mathcal{L}(\nu) \;\geq\; \mathcal{L}(\mu) \;+\; \langle \nabla\mathcal{L}(\mu),\, \nu - \mu \rangle \;+\; \frac{z}{2}\|\nu - \mu\|^2.$$

In particular, $\mathcal{L}(\mu)$ has a unique global minimum μ^* corresponding to the true measure.

(3) *Boundedness of the stochastic gradient. At each observation step, the gradient estimate* $\mathbf{g}_k$ *(the negative gradient of the loss functional, computed based on a sample of a finite number of realizations* Δf *for the current region) has bounded variance. That is, there exists* $\sigma^2 < \infty$ *such that for any step k:*

$$\mathbb{E}\Big[\, \|\mathbf{g}_k - \nabla\mathcal{L}(\mu_k)\|^2 \,\Big|\, \mu_k \Big] \;\le\; \sigma^2,$$

where μ_k *is the current parameter value, and* $\nabla\mathcal{L}(\mu_k)$ *is the true gradient (over the full dataset). This condition ensures that random fluctuations in the gradient estimate are bounded and do not grow unbounded.*

(4) *Learning rate. A monotonically decreasing sequence of learning rates* $\{\eta_k\}_{k\ge 0}$ *is used, or a sufficiently small constant step size satisfying the convergence conditions of SGD (e.g.,* $\sum_k \eta_k = \infty$*,* $\sum_k \eta_k^2 < \infty$*, or* $\eta < 2/L$ *in the case of a constant step for a momentum method). In particular, it is assumed that the steps are small enough that each gradient step does not "overshoot" the minimum and ensures a monotonic average decrease in* $\mathcal{L}(\mu)$*.*

Theorem statement. *Under assumptions (1)–(4), the measure estimates produced by the algorithm converge to the true measure as the number of iterations and observations increases. Formally, let* $\mu^{(m)}(\alpha,\beta)$ *denote the measure estimate after the m-th epoch (a full pass over all local regions with parameter updates). Then as* $m \to \infty$*, we have almost sure convergence* $\mu^{(m)}(\alpha,\beta) \to \mu^*(\alpha,\beta)$ *(with probability 1), and convergence in expectation:* $\mathbb{E}[\|\mu^{(m)} - \mu^*\|^2] \to 0$*. In other words, the identification algorithm is consistent: With an unlimited increase in the number of experimental repetitions and training iterations, it is capable of approximating the true distribution of the Preisach operator measure arbitrarily closely.*

3.3. Convergence proof

Part 1: Consistency of local estimates.

According to assumption (1), for each fixed local region (cell), the random observations of the output jump $\Delta f_{i,j}$ are independent and have a finite mean $E[\Delta f_{i,j}] = \mu^*_{ij}$, which corresponds to the true measure in that cell (since the jump magnitude is directly proportional to the cumulative contribution of all hysterons within that region). Repeating the experiment n times and averaging the results yields the estimate

$$\overline{\Delta f}^{(n)}_{i,j} = \frac{1}{n}\sum_{k=1}^{n} \Delta f^{(k)}_{i,j}.$$

By the law of large numbers, as $n \to \infty$, this estimate converges to the expected value:

$$\overline{\Delta f}^{(n)}_{i,j} \xrightarrow[n\to\infty]{} E[\Delta f_{i,j}] = \mu^*_{ij}.$$

Moreover, due to the independence of observations, the convergence can be regarded as uniform across all cells for a fixed partition (since the domain is discrete, and the finite union of converging sequences also converges). Thus, a sufficiently large number of repeated measurements ensures an arbitrarily small statistical error in estimating the measure in each individual cell. This justifies the validity of the objective function $\mathcal{L}(\mu)$ – for large sample sizes, it is minimized precisely at the point $\mu = \mu^*$.

Part 2: Properties of the loss function.

Assumption (2) ensure convexity of the minimization problem and uniqueness of the solution. Indeed, strong convexity of the functional $\mathcal{L}(\mu)$ implies that the equation $\nabla\mathcal{L}(\mu) = 0$ has a unique solution μ^*, which is a global minimum. Intuitively, the error surface $\mathcal{L}$ is bowl-shaped and lacks local minima, so any gradient-based method (even a stochastic one) should ultimately converge to the "bottom" of this bowl. The Lipschitz continuity of the gradient guarantees that the function is not excessively steep, and thus, the gradient descent step size can be chosen large enough without risking divergence; formally, for a step size $\eta < 2/L$, we ensure a monotonic decrease of $\mathcal{L}(\mu)$ at each iteration of standard gradient descent.

Part 3: Convergence of SGD.

The algorithm updates the measure parameters according to the SGD rule (Robbins-Monro):

$$\mu_{k+1} = \mu_k - \eta_k \, \mathbf{g}_k,$$

where $\mathbf{g}_k$ is the estimated gradient of the functional $\mathcal{L}$ at step k, computed based on a random subsample of data (in our case, a single local observation or a batch of observations for the current cell). In our algorithm, each such step corresponds to processing one cell and updating the corresponding parameter μ_{ij}.

From assumption (3), it follows that $\mathbf{g}_k$ is an unbiased estimator of the gradient:

$$\mathbb{E}[\mathbf{g}_k \mid \mu_k] = \nabla\mathcal{L}(\mu_k),$$

and its deviation around the true gradient is bounded by a variance σ^2. These are standard assumptions in the theory of SGD convergence.

Here, we outline the key idea. Consider the distance from the current estimate to the optimum, for instance, the squared deviation

$$D_k = \|\mu_k - \mu^*\|^2.$$

Let us write its change after one step of the method:

$$D_{k+1} = \|\mu_{k+1} - \mu^*\|^2 = \|\mu_k - \mu^* - \eta_k \mathbf{g}_k\|^2.$$

Expanding the squared norm and taking the expectation, we get

$$\mathbb{E}[D_{k+1} \mid \mu_k] = \|\mu_k - \mu^*\|^2 - 2\eta_k \, \mathbb{E}[\langle \mathbf{g}_k, \mu_k - \mu^* \rangle \mid \mu_k] + \eta_k^2 \, \mathbb{E}[\|\mathbf{g}_k\|^2 \mid \mu_k].$$

Given the unbiasedness of $\mathbf{g}_k$, we have

$$\mathbb{E}[\langle \mathbf{g}_k, \mu_k - \mu^* \rangle] = \langle \nabla\mathcal{L}(\mu_k), \mu_k - \mu^* \rangle.$$

Strong convexity yields the lower bound

$$\langle \nabla\mathcal{L}(\mu_k), \mu_k - \mu^* \rangle \geq z \, \|\mu_k - \mu^*\|^2,$$

since the gradient at μ_k points toward the optimum and cannot be too small relative to the distance (roughly, deviation from the optimum causes the function to grow at least as $z\|\mu_k - \mu^*\|^2/2$, which implies this inequality).

Moreover, bounded variance implies

$$\begin{aligned}\mathbb{E}[\|\mathbf{g}_k\|^2] &= \|\nabla\mathcal{L}(\mu_k)\|^2 + \mathbb{E}[\|\mathbf{g}_k - \nabla\mathcal{L}(\mu_k)\|^2] \\ &\leq \|\nabla\mathcal{L}(\mu_k)\|^2 + \sigma^2.\end{aligned}$$

And the Lipschitz condition on the gradient implies

$$\begin{aligned}&\|\nabla\mathcal{L}(\mu_k)\| \leq L\,\|\mu_k - \mu^*\| \\ \Rightarrow\quad &\|\nabla\mathcal{L}(\mu_k)\|^2 \leq L^2\,\|\mu_k - \mu^*\|^2.\end{aligned}$$

Substituting these estimates, we obtain:

$$\mathbb{E}[D_{k+1} \mid \mu_k] \leq \|\mu_k - \mu^*\|^2 - 2\eta_k z\,\|\mu_k - \mu^*\|^2 + \eta_k^2(L^2\,\|\mu_k - \mu^*\|^2 + \sigma^2).$$

This inequality describes the expected evolution of the error across iterations. Choose the step size η_k sufficiently small, e.g.,

$$\eta_k \leq \min\left\{\frac{1}{L}, \frac{z}{L^2}\right\} \quad \text{for all } k,$$

(which will be satisfied eventually if the step sizes decrease). Then the coefficient at $\|\mu_k - \mu^*\|^2$ becomes negative:

$$1 - 2\eta_k z + \eta_k^2 L^2 \approx 1 - 2\eta_k z + O(\eta_k^2) < 1,$$

for sufficiently small η_k. Ignoring the noise term $\eta_k^2\sigma^2$ (or accounting for the fact that it is summable under a fast enough decaying schedule), we see that on average,

$$D_{k+1} \leq q_k D_k, \quad \text{with some } q_k < 1.$$

Intuitively, this means each expected update brings the parameters closer to the optimum by a fraction of approximately $1 - \eta_k z$. In the limit as $k \to \infty$ (and $\eta_k \to 0$), the sequence $\{\mu_k\}$ converges to μ^*, as the distance to the optimum decreases geometrically (or at least sub-geometrically with variable step size). More formally, iterating the inequality and summing telescopically yields convergence in expectation:

$$\mathbb{E}[D_m] \leq D_0 \prod_{k=0}^{m-1} q_k + (\text{small residual term}).$$

Under a suitable decaying step size, we have $\prod_{k=0}^{\infty} q_k = 0$, hence

$$\lim_{m\to\infty} \mathbb{E}[\|\mu^{(m)} - \mu^*\|^2] = 0.$$

By a standard argument (see the Robbins–Monro theorem [48, 49, 62]), this implies almost sure convergence:

$$\mu^{(m)} \to \mu^* \quad \text{with probability 1.}$$

Thus, the stochastic gradient algorithm for minimizing $\mathcal{L}(\mu)$ is guaranteed to converge to the global minimum under the stated assumptions, i.e., to the true measure μ^*. In the context of the Preisach operator identification problem, this means that given an unlimited number of output observations and a sufficient number of training iterations, we can reconstruct the true hysteron distribution on the threshold plane with arbitrary accuracy. The computational experiments conducted by the authors confirm the method's effectiveness: high accuracy was achieved within just a few dozen iterations, even in the presence of stochasticness in the hysteron parameters.

4. Influence of threshold distribution on convergence

Let us examine how the properties of the distribution of hysteron thresholds affect the behavior of the described algorithm. The assumptions of the theorem require only finite variance and independence of threshold values, which are satisfied by most standard distributions (uniform, normal, beta distribution, etc.). Consequently, the theoretical convergence of the algorithm does not depend on the specific form of the distribution—be it uniform or normal—as both fulfill the conditions of the law of large numbers and bounded variance, thereby ensuring the validity of the presented proof. The algorithm is guaranteed to converge to the true measure for any threshold distribution satisfying these general conditions (including non-linear "quadratic" densities as used in the authors' experiments).

However, the type of distribution can affect the convergence rate and statistical accuracy when only a finite number of trials is available. Intuitively, this relates to how uniformly the hysterons are distributed across the domain and the degree of response variability in different regions.

- If the threshold values are uniformly distributed over the domain (without pronounced clustering), then the contribution of the measure in each local cell will be of comparable magnitude. This implies that during scanning, each cell generates an output signal Δf of similar scale. The measurement noise (i.e., variation in Δf across trials) will also be similar across regions. As a result, the algorithm will learn in a more or less uniform manner over the plane: no area will require significantly more repetitions than others to achieve a given accuracy. One may say that with a uniform threshold distribution, the condition number of the problem (signal-to-noise ratio across cells) is approximately constant.
- If the threshold distribution is non-uniform, e.g., it has one or several peaks (as in a normal distribution concentrated around the mean or a multimodal distribution), then different regions will contain varying numbers of hysterons. In regions with high hysteron density, the output jump Δf will, on average, be larger, and statistical estimation will become reliable with relatively few repetitions (high signal, noise averages out). Conversely, in regions where the hysteron density is low (e.g., at the tails of a normal distribution), the expected output change is very small—many trials may result in no switching at all. Accurate estimation of the tiny value μ_{ij} in such regions may require a greater number of trials. In other words, the signal-to-noise ratio is worse there, and the variance of the relative error is higher. As a result, the algorithm may converge non-uniformly: quickly in cells where the threshold distribution yields a strong signal, and more slowly in cells with sparse hysterons. Nevertheless, in the limit of a large number of trials, all regions will be learned to the required precision; the differences manifest only in convergence speed and intermediate accuracy at finite iterations.
- The support range of the distribution also plays a role. If the threshold distribution has wide support (e.g., uniform over a large interval or normal with large variance), then there exist very high thresholds β and very low ones α that occur rarely. For correct identification of the measure at the edges of the triangular domain, the input signal must cover the entire range (i.e., $\beta_{\max}$ must not be less than the highest possible threshold). If the distribution has extremely long tails, the system may need to be nearly saturated—but in real-world applications, the range of input signals is usually limited. Hence, it is typically assumed that the threshold distribution has compact support or, at least, negligible mass in the infinite tails. In our considerations, we assume that the maximum and minimum thresholds are finite and known, such that the algorithm can cover the

full probability range of the distribution. If the threshold distribution is narrow (e.g., normal with small variance, concentrated around a particular value), then the task is simplified—the hysterons are clustered, and their measure is concentrated in a few cells. The algorithm will rapidly identify these high-density regions and adjust the measure accordingly. The remaining (practically empty) regions are also correctly identified—their measure is close to zero, and a few trials are sufficient to confirm the absence of significant hysteron activity.

5. Computational experiment

To illustrate the proposed method, let us consider the distribution of the measure for weekly relays obtained in [58] from real data for the classical Preisach operator. In the framework of the computational experiment, the Preisach operator was approximated by a discrete model with 800 hysterons, uniformly distributed on the plane $\beta > \alpha$. It was assumed that the threshold numbers were stochastic variables with a quadratic probability density function:

$$f_X(x) = \begin{cases} 0, & \forall x \notin [x_0 - \delta, x_0 + \delta], \\ k\,(x - x_0)^2 + y_0, & \forall x \in [x_0 - \delta, x_0 + \delta], \end{cases}$$

where x_0 is the center of the distribution, δ is the width of the distribution, k, y_0 are the characteristics of the distribution, chosen such that $\int_a^b f(x)dx = 1$. The boundaries of the distributions of neighboring hysterons overlapped by 20%, as shown in Figure 6.

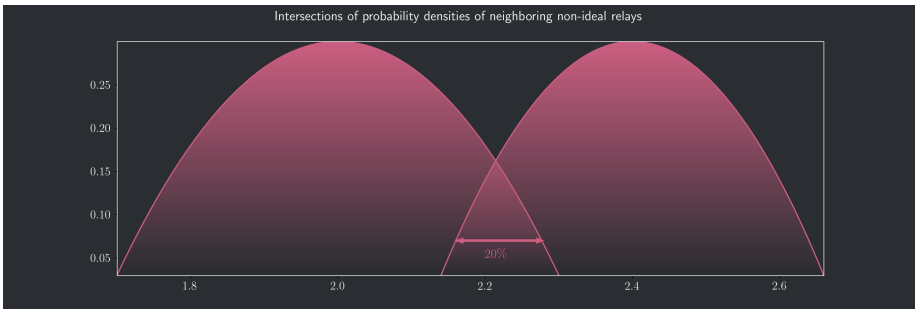

Figure 6. Visualization of probability densities for neighboring non-ideal relays.

To estimate the expected value (2.2) for each local area (α_i, β_j), 40 observations were conducted in each epoch (an epoch is defined as one complete pass through all local areas of the Preisach operator's measure). The training dynamics over 12 epochs are presented in Figure 7.

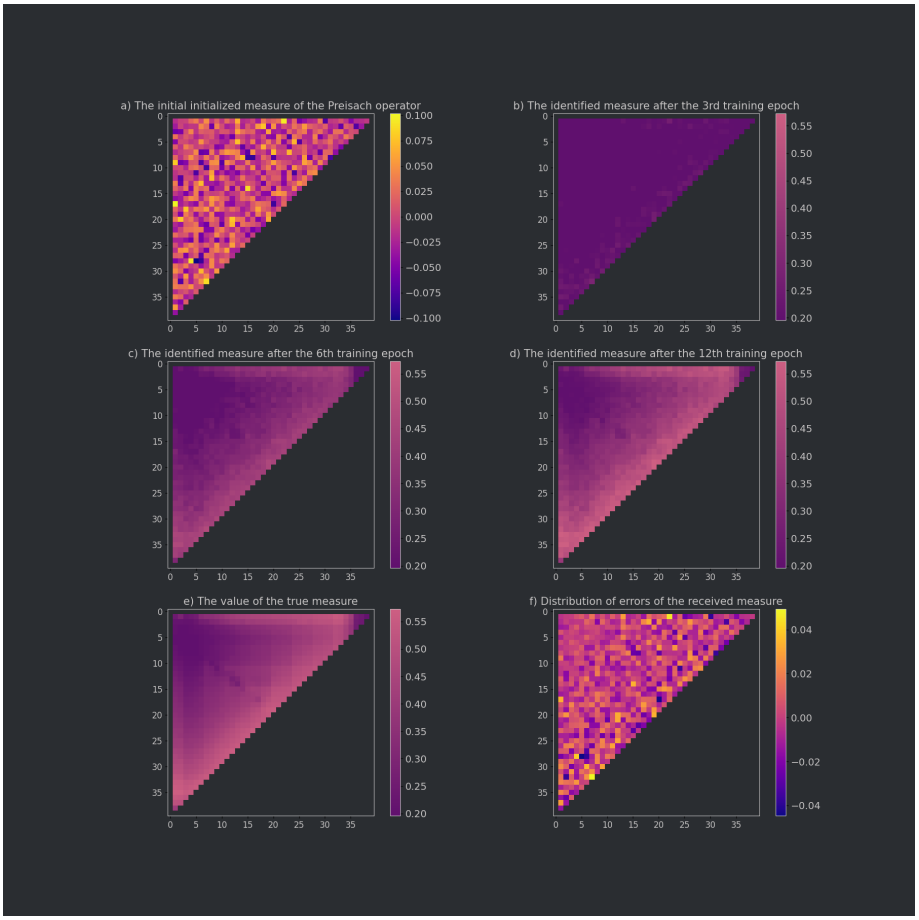

Figure 7. Numerical experiment: a) initial measure initialization in the model, b) measure value of the operator after 3 epochs of training, c) measure value of the operator after 6 epochs of training, d) measure value of the operator after 12 epochs of training, e) true measure value, and f) error distribution.

6. Stopping criterion for Preisach measure identification

The choice of stopping criterion in identifying the Preisach measure distribution depends significantly on the characteristics of the underlying distribution and the measurement noise level.

6.1. Influence of hysteron parameter distribution

The geometry of the optimization landscape for the Preisach measure $\mu(\alpha,\beta)$ strongly depends on its parameter distribution:

- If the measure is concentrated in specific regions of the (α,β) parameter plane, the optimization typically encounters a simpler loss landscape with clearly defined minima, allowing rapid convergence. In such scenarios, the gradient norm decreases swiftly upon identifying dominant regions, thus justifying the use of a relatively aggressive stopping threshold.

- Conversely, if the distribution is broad or multimodal, the optimization may become significantly more complex. The loss landscape can exhibit extended plateaus or several shallow minima corresponding to different aspects of the distribution. Here, training often shows intermittent phases: rapid error reduction as major distribution regions are identified, followed by plateaus before further improvement occurs. It is essential to distinguish between genuine convergence plateaus and false plateaus—temporary stagnation after fitting prominent distribution features but before fully capturing subtle aspects. Thus, complex or multimodal distributions require more conservative stopping criteria, such as smaller gradient thresholds ε and longer patience to ensure the algorithm comprehensively explores the parameter space and accurately captures the full structure.

In summary, complex hysteron distributions generally demand stricter stopping criteria to confirm thorough convergence, whereas simpler distributions permit earlier stopping once the dominant features are learned.

6.2. Effect of measurement noise

Measurement noise and finite sampling introduce stochasticity in Preisach measure identification, affecting the optimal stopping criterion:

- High noise levels set practical limits on achievable accuracy, as continued training beyond a certain threshold increasingly fits noise rather than the actual underlying signal. The training loss typically reaches a "noise floor," beyond which improvements are minimal and likely to be artifacts of random noise.
- Under significant noise, the gradient norm $\|\nabla L\|$ will not diminish indefinitely but instead oscillate around a baseline value determined by noise intensity. Consequently, stopping criteria must accommodate this behavior by setting gradient thresholds above this baseline. For example, if gradient norms fluctuate around 10^{-3}, it is advisable to select a threshold such as 5×10^{-3}, acknowledging that smaller gradients represent indistinguishable noise rather than meaningful optimization progress.
- Conversely, when measurement noise is low, allowing the model to achieve near-zero loss, stricter stopping criteria can leverage the higher data precision to refine the model more thoroughly.

6.3. Balancing overfitting and underfitting

In Preisach measure identification, avoiding overfitting—fitting noise or irrelevant dynamics rather than the true underlying distribution—is crucial. A carefully selected stopping criterion acts as an implicit regularizer:

- High noise conditions increase the risk of overfitting with prolonged training. Thus, an earlier stopping guided by validation metrics or plateau detection helps prevent mistaking noise for meaningful signal.
- Conversely, excessively early stopping risks underfitting, resulting in incomplete identification of the measure's significant features. The ideal stopping point should balance these risks by correlating with the signal-to-noise ratio: typically, the residual training error should approach the magnitude of measurement noise.

- Incorporating domain knowledge aids this balance. For instance, recognizing that certain regions of the parameter space are negligible allows prioritizing computational resources on significant regions and avoiding unnecessary optimization in noisy regions.

6.4. Recommended stopping strategy

Considering optimization theory and empirical heuristics, the recommended stopping approach is to terminate iterative training upon reaching an ϵ-optimal solution, defined by a sufficiently small gradient norm (indicating first-order optimality) or when the loss curve flattens substantially. The parameter ϵ should reflect both the experimental noise level and the complexity of the underlying Preisach measure. This ensures that the measure is identified accurately without risking overfitting or wasting computational resources through over-training. Such an approach is supported by both theoretical convergence properties of stochastic optimization algorithms (e.g., SGD, Adam, AMSGrad) and empirical evidence showing limited gains from additional training beyond an optimal stopping point.

7. Conclusions

In this work, a method for identifying the measure of a stochastic Preisach operator is proposed, based on the step-by-step reconstruction of the measure on the plane of threshold parameter numbers. The algorithm is based on the sequential application of specific input signals that trigger switching only in certain elementary hysterons within specified local areas. Repeated application of such input stimuli and the use of machine learning methods allow for the effective estimation of the expected changes in the state of the hysterons and the reconstruction of the operator's measure from experimental data.

The conducted computational experiment confirmed the effectiveness of the proposed approach. The use of SGD and partial optimization of the measure parameters in each local area ensured the convergence of the algorithm and high accuracy in recovering the true distribution of the measure, even in the presence of stochasticity in the hysteron parameters.

In the future, it is planned to examine in more detail the limitations and possibilities for generalizing the proposed method. Particularly relevant is the investigation of the influence of various distributions of hysteron threshold numbers on the convergence and accuracy of the identification algorithm. A possible direction for development is the extension of the method to more complex distributions of threshold numbers, as well as the consideration of correlated stochastic parameters.

Additionally, attention should be paid to optimizing the computational costs of the algorithm when working with high-dimensional models and a large number of hysterons. The development of adaptive algorithms capable of efficiently operating in real-time and processing large volumes of data will allow the method to be applied to a wide range of practical tasks related to the modeling and control of systems with hysteresis.

Thus, the proposed method for identifying the measure of a stochastic Preisach operator opens up new possibilities for modeling and analyzing complex systems with hysteresis properties, and further research in this direction may significantly enhance the efficiency and accuracy of describing hysteresis phenomena in various fields of science and engineering.

Use of Generative-AI tools declaration

The authors declare they have not used Artificial Intelligence (AI) tools in the creation of this article.

Conflict of interest

The authors declare no conflicts of interest.

References

1. R. Abdolvand, H. M. Lavasani, G. K. Ho, F. Ayazi, Thin-film piezoelectric-on-silicon resonators for high-frequency reference oscillator applications, *IEEE Transactions on Ultrasonics, Ferroelectrics, and Frequency Control*, **55** (2008), 2596–2606. https://doi.org/10.1109/TUFFC.2008.976
2. F. Baronti, N. Femia, R. Saletti, C. Visone, W. Zamboni, Hysteresis modeling in Li-ion batteries, *IEEE Trans Magn.*, **50** (2014), 1–4. https://doi.org/10.1109/TMAG.2014.2323426
3. F. Baronti, N. Femia, R. Saletti, C. Visone, W. Zamboni, Preisach modelling of lithium-iron-phosphate battery hysteresis, *J. Energy Storage.*, **4** (2015), 51–61. https://doi.org/10.1016/j.est.2015.09.004
4. I. Bodale, A. Stancu, Reversible and irreversible processes in drying and wetting of soil, *Materials*, **13** (2019), 135. https://doi.org/10.3390/ma13010135
5. S. V. Borzunov, M. E. Semenov, N. I. Sel'vesyuk, P. A. Meleshenko, A. M. Solovyov, Stochastic model of a hysteresis converter with a domain structure, *Math. Model. Comput. Simul.*, **14** (2022), 305–321. https://doi.org/10.1134/S207004822202003X
6. S. V. Borzunov, M. E. Semenov, N. I. Sel'vesyuk, P. A. Meleshenko, Hysteretic converters with stochastic parameters, *Math. Model. Comput. Simul.*, **12** (2020), 164–175. https://doi.org/10.1134/S2070048220020040
7. M. Belhaq, A. Bichri, J. Der Hogapian, J. Mahfoud, Effect of electromagnetic actuations on the dynamics of a harmonically excited cantilever beam, *Int. J. Non-Linear Mech.*, **46** (2011), 828–833. https://doi.org/10.1016/j.ijnonlinmec.2011.03.001
8. L. Chen, Q. Yi, T. Ben, Z. Zhang, Y. Wang, Parameter identification of Preisach model based on velocity-controlled particle swarm optimization method, *AIP Adv.*, **11** (2021), 015022. https://doi.org/10.1063/9.0000030
9. G. Cipriani, M. Corpora, D. Curto, V. Di Dio, V. Franzitta, M. Trapanese, An electromagnetic generator for MAGLEV transportation systems, *2015 International Conference on Renewable Energy Research and Applications (ICRERA)*, 2015, 1523–1526. https://doi.org/10.1109/ICRERA.2015.7418662
10. P. Cacciola, A. Tombari, Steady state harmonic response of nonlinear soil-structure interaction problems through the Preisach formalism, *Soil Dyn. Earthq. Eng.*, **144** (2021), 106669. https://doi.org/10.1016/j.soildyn.2021.106669

11. P. Cacciola, I. Caliò, N. Fiorini, G. Occhipinti, D. Spina, A. Tombari, Seismic response of nonlinear soil-structure interaction systems through the Preisach formalism: the Messina Bell Tower case study, *Bull Earthquake Eng.*, **20** (2020), 3485–3514. https://doi.org/10.1007/s10518-021-01268-w
12. P. Chojecki, G. Walters, Z. Forrester, T. Nishida, Preisach modeling of imprint on hafnium zirconium oxide ferroelectric capacitors, *J. Appl. Phys.*, **130** (2021), 094102. https://doi.org/10.1063/5.0053185
13. D. Davino, P. Krejčí, A. Pimenov, D. Rachinskii, C. Visone, Analysis of an operator-differential model for magnetostrictive energy harvesting, *Commun. Nonlinear Sci. Numer. Simul.*, **39** (2016), 504–519. https://doi.org/10.1016/j.cnsns.2016.04.004
14. J. Dho, C. W. Leung, M. G. Blamire, Universal time relaxation behavior of the exchange bias in ferromagnetic/antiferromagnetic bilayers, *J. Appl. Phys.*, **99** (2006), 033910. https://doi.org/10.1063/1.2169876
15. D. Damjanovic, M. Demartin, Contribution of the irreversible displacement of domain walls to the piezoelectric effect in barium titanate and lead zirconate titanate ceramics, *J. Phys.: Condens. Matter.*, **9** (1997), 4943. https://doi.org/10.1088/0953-8984/9/23/018
16. B. Ducharne, B. Gupta, G. Litak, Simulation of synchronized-switching method energy harvester including accurate piezoceramic nonlinear behavior, *Energies*, **12** (2019), 4466. https://doi.org/10.3390/en12234466
17. R. Egli, VARIFORC: an optimized protocol for calculating non-regular first-order reversal curve (FORC) diagrams, *Global Planet. Change*, **110** (2013), 302–320. https://doi.org/10.1016/j.gloplacha.2013.08.003
18. X. Fan, K. Guo, Y. Wang, Toward a high performance and strong resilience wind energy harvester assembly utilizing flow-induced vibration: role of hysteresis, *Energy*, **251** (2022), 123921. https://doi.org/10.1016/j.energy.2022.123921
19. D. Flynn, A. Zhezherun, A. Pokrovskii, J. P. O'Kane, Modeling discontinuous flow through porous media using ODEs with Preisach operator, *Phys. B*, **403** (2008), 440–442. https://doi.org/10.1016/j.physb.2007.08.070
20. J. Freudenreich, *Étude de l'aimantation initiale en fonction de la température*, Ph.D. Thesis, ETH Zurich, 1918. https://doi.org/10.3929/ethz-a-000092325
21. C. Gavioli, P. Krejčí, Control and controllability of PDEs with hysteresis, *Appl. Math. Optim.*, **84** (2021), 829–847. https://doi.org/10.1007/s00245-020-09663-6
22. C. Gavioli, P. Krejčí, Phase transitions in porous media, *Nonlinear Differ. Equ Appl.*, **29** (2022), 72. https://doi.org/10.1007/s00030-022-00805-z
23. C. Gavioli, P. Krejčí, Degenerate diffusion with Preisach hysteresis, *arXiv*, 2023. https://doi.org/10.48550/arXiv.2303.17451
24. R. B. Gorbet, D. W. L. Wang, K. A. Morris, Preisach model identification of a two-wire SMA actuator, *Proceedings. 1998 IEEE International Conference on Robotics and Automation*, 1998, 2161-2167. https://doi.org/10.1109/ROBOT.1998.680641
25. V. Hassani, T. Tjahjowidodo, T. N. Do, A survey on hysteresis modeling, identification and control, *Mech. Syst. Signal Process*, **49** (2014), 209–233. https://doi.org/10.1016/j.ymssp.2014.04.012

26. R. J. Harrison, J. M. Feinberg, FORCinel: an improved algorithm for calculating first-order reversal curve distributions using locally weighted regression smoothing, *Geochem Geophys Geosyst.*, **9** (2008), 1–11. https://doi.org/10.1029/2008GC001987
27. Y. He, B. Bahr, M. Si, P. Ye, D. Weinstein, A tunable ferroelectric based unreleased RF resonator, *Microsyst Nanoeng.*, **6** (2020), 8. https://doi.org/10.1038/s41378-019-0110-1
28. K. H. Hoffmann, J. Sprekels, A. Visintin, Identification of hysteresis loops, *J. Comput. Phys.*, **78** (1988), 215–230. https://doi.org/10.1016/0021-9991(88)90045-9
29. D. C. Hughes, J. T. Wen, Preisach modeling and compensation for smart material hysteresis, *Act. Mater. Smart Struct.*, 1995, 50–64. https://doi.org/10.1117/12.200933
30. S. C. Hwang, C. S. Lynch, R. M. McMeeking, Ferroelectric/ferroelastic interactions and a polarization switching model, *Acta Metall. Mater.*, **43** (1995), 2073–2784. https://doi.org/10.1016/0956-7151(94)00379-V
31. S. Humad, R. Abdolvand, G. K. Ho, G. Piazza, F. Ayazi, High frequency micromechanical piezo-on-silicon block resonators, *IEEE International Electron Devices Meeting 2003*, 2003. https://doi.org/10.1109/IEDM.2003.1269437
32. R. V. Iyer, X. Tan, P. S. Krishnaprasad, Approximate inversion of the Preisach hysteresis operator with application to control of smart actuators, *IEEE Trans. Automat. Contr.*, **50** (2005), 798–810. https://doi.org/10.1109/TAC.2005.849205
33. R. V. Iyer, M. E. Shirley, Hysteresis parameter identification with limited experimental data, *IEEE Trans. Magn.*, **40** (2024), 3227–3239. https://doi.org/10.1109/TMAG.2004.833427
34. D. C. Jiles, D. L. Atherton, Theory of ferromagnetic hysteresis (invited), *J. Appl. Phys.*, **55** (1984), 2115–2120. https://doi.org/10.1063/1.333582
35. T. Kalmár-Nagy, A. Amann, D. Kim, D. Rachinskii, The devil is in the details: spectrum and eigenvalue distribution of the discrete Preisach memory model, *Commun. Nonlinear Sci. Numer. Simul.*, **77** (2019), 1–17. https://doi.org/10.1016/j.cnsns.2019.04.023
36. V. Khikhlovskyi, A. V. Gorbunov, A. J. J. M. van Breemen, R. A. J. Janssen, G. H. Gelinck, M. Kemerink, Multi-bit organic ferroelectric memory, *Org. Electron.*, **14** (2013), 3399–3405. https://doi.org/10.1016/j.orgel.2013.09.006
37. P. Krejčí, E. Rocca, J. Sprekels, Unsaturated deformable porous media flow with thermal phase transition, *Math. Mod. Meth. Appl. Sci.*, **27** (2017), 2675–2710. https://doi.org/10.1142/S0218202517500555
38. P. Krejčí, Evolution variational inequalities and multidimensional hysteresis operators, In: *Nonlinear differential equations*, Boca Raton: Chapman and Hall/CRC, 2024.
39. H. J. Khasawneh, Z. S. Abo-Hammour, M. I. Al Saaideh, S. M. Momani, Identification of hysteresis models using real-coded genetic algorithms, *Eur. Phys. J. Plus.*, **134** (2019), 507. https://doi.org/10.1140/epjp/i2019-12883-7
40. C. E. Korman, I. D. Mayergoy, Review of Preisach type models driven by stochastic inputs as a model for after-effect, *Phys. B*, **233** (1997), 381–389. https://doi.org/10.1016/S0921-4526(97)00325-6
41. M. A. A. Krasnosel'skii, A. V. Pokrovskii, *Systems with hysteresis*, Berlin: Springer, 2012.

42. J. Li, H. Huang, T. Morita, Stepping piezoelectric actuators with large working stroke for nano-positioning systems: a review, *Sens. Actuators A: Phys.*, **292** (2019), 39–51. https://doi.org/10.1016/j.sna.2019.04.006

43. G. Litak, J. Margielewicz, D. Gaska, A. Rysak, C. Trigona, On theoretical and numerical aspects of bifurcations and hysteresis effects in kinetic energy harvesters, *Sensors*, **22** (2022), 381. https://doi.org/10.3390/s22010381

44. I. D. Mayergoyz, "Dynamic Preisach models of hysteresis", *IEEE Trans. Magn.*, **24** (1988), 2925–2927. https://doi.org/10.1109/20.92290

45. I. D. Mayergoyz, *Mathematical models of hysteresis and their applications*, Academic Press, 2003. https://doi.org/10.1016/B978-0-12-480873-7.X5000-2

46. I. D. Mayergoyz, Mathematical models of hysteresis, *IEEE Trans. Magn.*, **22** (1986), 603–608. https://doi.org/10.1109/TMAG.1986.1064347

47. P. Muralt, Ferroelectric thin films for micro-sensors and actuators: a review, *J. Micromech. Microeng.*, **10** (2000), 1366. https://doi.org/10.1088/0960-1317/10/2/307

48. Y. Nesterov, *Lectures on convex optimization,* Berlin: Springer, 2018. https://doi.org/10.1007/978-3-319-91578-4

49. A. Nemirovski, A. Juditsky, G. Lan, A. Shapiro, Robust stochastic approximation approach to stochastic programming, *SIAM J. Optim.*, **19** (2009), 1574–1609. https://doi.org/10.1137/070704277

50. S. O'Ceallaigh, A. Pimenov, A. Pokrovskii, D. Rachinskii, A. Zhezherun, Algorithm for linear stability analysis in systems with Preisach hysteresis, *Phys. B*, **403** (2008), 305–307. https://doi.org/10.1016/j.physb.2007.08.035

51. J. Ortiz-Lopez, F. Luty, Optical studies of thermal cycling and hysteresis effects in elastic order-disorder phase transformations. I. Pure alkali-metal cyanide crystals, *Phys. Rev. B*, **37** (1988), 5452. https://doi.org/10.1103/physrevb.37.5452

52. F. Preisach, Über die magnetische Nachwirkung, *Z. Phys.*, **94** (1935), 277–302. https://doi.org/10.1007/BF01349418

53. C. R. Pike, A. P. Roberts, K. L. Verosub, First order reversal curve diagrams and thermal relaxation effects in magnetic particles, *Geophys. J. Int.*, **145** (2001), 721–730. https://doi.org/10.1046/j.0956-540x.2001.01419.x

54. A. Poulovassilis, The effect of the entrapped air on the hysteresis curves of a porous body and on its hydraulic conductivity, *Soil Sci.*, **109** (1970), 154–162.

55. G. Quaranta, W. Lacarbonara, S. F. Masri, A review on computational intelligence for identification of nonlinear dynamical systems, *Nonlinear Dyn.*, **99** (2020), 1709–1761. https://doi.org/10.1007/s11071-019-05430-7

56. M. Ruderman, On stability of linear dynamic systems with hysteresis feedback, *Math. Model. Nat. Phenom.*, **15** (2020), 52. https://doi.org/10.1051/mmnp/2020014

57. S. Ruta, O. Hovorka, P. W. Huang, K. Wang, G. Ju, R. Chantrell, First order reversal curves and intrinsic parameter determination for magnetic materials; limitations of hysteron-based approaches in correlated systems, *Sci. Rep.*, **7** (2017), 45218. https://doi.org/10.1038/srep45218

58. R. Roussel, A. Edelen, D. Ratner, K. Dubey, J. P. Gonzalez-Aguilera, Y. K. Kim, et al., Differentiable Preisach modeling for characterization and optimization of particle accelerator systems with hysteresis, *Phys. Rev. Lett.*, **128** (2022), 204801. https://doi.org/10.1103/physrevlett.128.204801

59. L. A. Rios, D. Rachinskii, R. Cross, A model of hysteresis arising from social interaction within a firm, *J. Phys.: Conf. Ser.*, **811** (2017), 012011. https://doi.org/10.1088/1742-6596/811/1/012011

60. J. B. Restorff, H. T. Savage, A. E. Clark, M. Wun-Fogle, Preisach modeling of hysteresis in Terfenol, *J. Appl. Phys.*, **67** (1990), 5016–5018. https://doi.org/10.1063/1.344708

61. A. Stancu, C. Pike, L. Stoleriu, P. Postolache, Micromagnetic and Preisach analysis of the first order reversal curves (FORC) diagram, *J. Appl. Phys.*, **93** (2003), 6620–6622. https://doi.org/10.1063/1.1557656

62. S. Shalev-Shwartz, O. Shamir, N. Srebro, K. Sridharan, Stochastic convex optimization, *Proceedings of the 22nd Annual Conference on Learning Theory (COLT 2009)*, 2009.

63. M. E. Semenov, S. V. Borzunov, P. A. Meleshenko, A. V. Lapin, A model of optimal production planning based on the hysteretic demand curve, *Mathematics*, **10** (2022), 3262. https://doi.org/10.3390/math10183262

64. M. E. Semenov, O. O. Reshetova, S. V. Borzunov, P. A. Meleshenko, Self-oscillations in a system with hysteresis: the small parameter approach, *Eur. Phys. J. Spec. Top.*, **230** (2021), 3565–3571. https://doi.org/10.1140/epjs/s11734-021-00237-3

65. M. E. Semenov, S. V. Borzunov, P. A. Meleshenko, A new way to compute the Lyapunov characteristic exponents for non-smooth and discontinues dynamical systems, *Nonlinear Dyn.*, **109** (2022), 1805–1821. https://doi.org/10.1007/s11071-022-07492-6

66. M. E. Semenov, S, V. Borzunov, P. A. Meleshenko, Stochastic Preisach operator: definition within the design approach, *Nonlinear Dyn.*, **101** (2020), 2599–2614. https://doi.org/10.1007/s11071-020-05907-w

67. M. E. Semenov, S. V. Borzunov, P. A. Meleshenko, N. I. Sel'vesyuk, The Preisach model of hysteresis: fundamentals and applications, *Phys Scr.*, **99** (2024), 062008. https://doi.org/10.1088/1402-4896/ad4aa2

68. M. Sjöström, D. Djukic, B. Dutoit, *Parametrised Preisach modelling of hysteresis in high temperature superconductors*, 1998.

69. E. C. Stoner, E. P. Wohlfarth, A mechanism of magnetic hysteresis in heterogeneous alloys, *Philos. Trans. R. Soc. Lond. Ser. A, Math. Phys. Sci.*, **240** (1948), 599–642. https://doi.org/10.1098/rsta.1948.0007

70. M. Trapanese, Identification of the parameters of reduced vector Preisach model by neural networks, *IEEE Trans. Magn.*, **44** (2008), 3197–3200. https://doi.org/10.1109/tmag.2008.2001657

71. I. Urbanavičiūtė, T. D. Cornelissen, X. Meng, R. P. Sijbesma, M. Kemerink, Physical reality of the Preisach model for organic ferroelectrics, *Nat. Commun.*, **9** (2018), 4409. https://doi.org/10.1038/s41467-018-06717-w

72. P. Venegas, D. Gómez, M. Arrinda, M. Oyarbide, H. Macicior, A. Bermúdez, Kalman filter and classical Preisach hysteresis model applied to the state of charge battery estimation, *Comput. Math. Appl.*, **118** (2022), 74–84. https://doi.org/10.1016/j.camwa.2022.05.009

73. Z. Yang, S. Zhou, J. Zu, High-performance piezoelectric energy harvesters and their applications, *Joule*, **2** (2018), 642–697. https://doi.org/10.1016/j.joule.2018.03.011

74. L. Yang, B. Ding, W. Liao, Y. Li, Identification of Preisach model parameters based on an improved particle swarm optimization method for piezoelectric actuators in micro-manufacturing stages, *Micromachines*, **13** (2022), 698. https://doi.org/10.3390/mi13050698

75. Y. Yu, N. Naganathan, R. Dukkipati, Preisach modeling of hysteresis for piezoceramic actuator system, *Mech. Mach. Theory*, **37** (2002), 49–59. https://doi.org/10.1016/S0094-114X(01)00065-9

76. K. Zhang, T. Zhao, H. Fujiwara, Training effect of exchange biased iron-oxide/ferromagnet systems, *J. Appl. Phys.*, **89** (2001), 6910–6912. https://doi.org/10.1063/1.1360682

AIMS Press